IN-PLANE ENERGY ABSORPTION AND DEFORMATION PATTERNS OF RE-ENTRANT AUXETIC CRASH BOX

ARIF ROCHMAN FACHRUDIN[1,2], MOCH. AGUS CHOIRON[3], ANINDITO PURNOWIDODO[3], YUDY SURYA IRAWAN[3]

[1]Doctoral Student of Mechanical Engineering Department, Brawijaya University, Indonesia

[2]Mechanical Engineering, State Polytechnic of Malang, Indonesia

[3]Mechanical Engineering Department, Brawijaya University, Indonesia

DOI: 10.17973/MMSJ.2025_03_2025002

E-mail to corresponding author: agus_choiron@ub.ac.id

This article presents the crush response of a re-entrant auxetic square tube under quasi-static compressive loading. Re-entrant auxetic-filled tubes are compared with an empty square tube, with the auxetic structures fabricated using a 3D printing technique. Experimental and simulation results demonstrate good agreement, confirming that the addition of re-entrant auxetic structures significantly improves the crashworthiness performance of the crash tube compared to an empty tube. By analyzing the experimental energy absorption (EA) values, the inclusion of a re-entrant auxetic square tube resulted in a 53.047% increase in energy absorption compared to the empty tube.

KEYWORDS

energy absorption, auxetic, re-entrant, square tube, 3D printing, quasi-static

1 INTRODUCTION

Vehicle manufacturers in the automotive industry continue to develop good quality vehicles in terms of performance and safety. The study of crashworthiness is an important research subject due to manufacturers develop safe vehicles by preventing serious injury to passengers in the event of a vehicle accident. A car's crashworthiness refers to a car's ability to withstand the impact of a collision and protect the driver and passengers. This relates to vehicle safety standards tested and regulated by transportation authorities in various countries. One of the passive safety devices used to absorb kinetic energy in cars is the crash box, located between the main structure and the bumper (Abdullah et al., 2020). The crash box installed in a vehicle refers to a thin-wall structure made of metal or composite material that is fixed or mounted at the frontal area of the vehicle. The structure serves as an energy-absorbing member to the vehicle due to collision in the event of a crash (Hussain et al., 2017). If the impact force exerted on the columns cannot be sufficiently absorbed, it is transferred directly to the passenger cabin during collision. This may cause fatal injury to the passengers and damage to the vehicle. In general, the energy absorption effect of the crash box is closely related to the shape (Velmurugan & Muralikannan, 2009), outer cross-sectional design and inner filling structure of the crash box (Xiao et al., 2016)(K. Wang et al., 2022).. All the improvements in crashworthiness can be done by working on new geometric designs or using innovative materials for safety components (Boreanaz & Belingardi, 2018).

The research on the crash box filler structure was initially made with a simpler structure. The development of 3D printing capabilities produces more complex geometry, hence manufactured crash box filler structures easier and faster. The 3D printing technology gave new ideas to the design of crash box structure. (Li et al., 2019). Some variations in the filler structure include thickness (Fang et al., 2015), number of structures (K. Wang et al., 2022)(Astuti et al., 2023), material (J. Wang et al., 2020)(Song et al., 2022) and the angle of the filler structure (Ghiasvand et al., 2023)(Dhari et al., 2021). The crash box design with 3D printed lattice filler has better energy absorption capabilities than without a filler structure (Simpson & Kazancı, 2020).

The development of the shape and structure of the crash box design has been inspired by nature, one of these designs is using an auxetic structure (Dhari et al., 2021) as a filling structure. Auxetic structures have a negative Poisson's ratio (NPR)(Warner et al., 2017)(Meena & Singamneni, 2019). It is designed that can expand when pulled and shrink when pressed (Ghiasvand et al., 2023). This allows the auxetic crash box to absorb kinetic energy during a crash more effectively and with controlled deformation (Mauko et al., 2021). The auxetic structure of the lattice has a relatively higher density and exhibits higher reaction forces and high energy absorption. The deformation characteristics are counter-intuitive, giving auxetic materials a higher shear modulus, increased indentation resistance (X. T. Wang et al., 2017), high energy absorption (Rad, 2015), explosion resistance, increased fracture toughness, synclastic behavior, acoustic dampening and other extraordinary properties (H. Liu et al., 2021). Materials and structures that exhibit negative Poisson's ratio (NPR) can be used to further improve the feasibility of these TW (Thin Wall) structures. NPR material will contract transversely when compressed axially and conversely will expand transversely when expanded (Evans, 1991) Auxetic materials with a negative Poisson's ratio can absorb high energy during impacts (Airoldi et al., 2020)(Zhao et al., 2018)(Yang & Ma, 2021).

In auxetic crash box design, the internal structure or core of the crash box is usually created using a re-entrant pattern or geometric pattern that has reshaped corners. This pattern helps distribute the energy generated during an accident more evenly, thereby increasing the crash box's ability to absorb energy and protect passengers and vehicle components (Shruti et al., 2020). Several studies have used re-entrant structures as filler materials due to their good energy absorption capabilities (W. Liu et al., 2016)(Lian & Wang, 2023)(Günayd et al., 2019)(Huang et al., 2017)(Ju & Summers, 2011).

The interaction between the crash tubes and filler structures plays an important role in enhancing the energy absorption behavior of the structure. The majority of researchers were working on filling the square tubes with conventional foam or lattice structures. Auxetic lattice types have only received limited attention despite their advantageous properties. Therefore, more investigation is conducted to understand the potential of the material. However, the number of studies on such lattices has been limited making it worthwhile to be considered for further investigations.

The aim of this study is to investigate deformation behavior and the crashworthiness performance of re-entrant auxetic within square tubes of the square under quasi-static compressive loading. An experimental study has been performed and combined with finite element modeling for the analysis of

auxetic filler structures within thin-walled tubes subjected to quasi-static compression.

2 METHODOLOGY

This study was to investigate and compare the energy absorption capabilities of an empty tube to that of one filled with a structural re-entrant auxetic. A commonly available square profile tube has been selected with a cross-sectional geometry of 76.2 x 76.2 mm, as presented in Figure 1. A wall thickness of 1.9 mm and an overall tube length of 150 mm were selected. The selected tube material is Aluminium 6063.

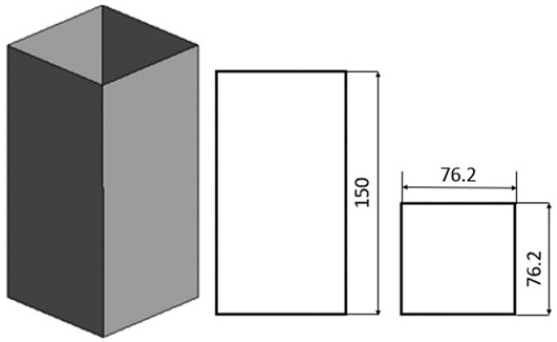

Figure 1. Square Tube geometry (a) isometric, (b) front, and (c) top view (unit in mm)

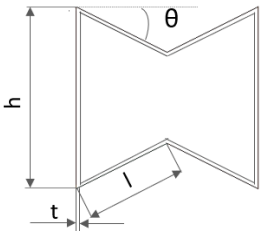

Figure 2. Geometric configuration of re-entrant auxetic cells

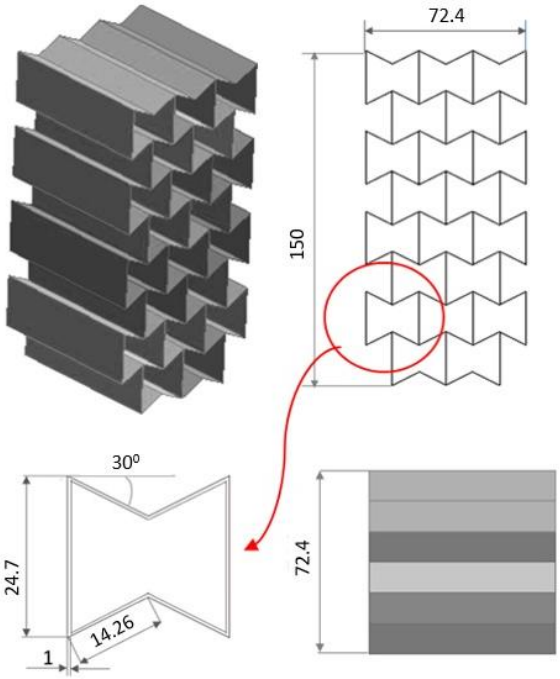

Figure 3. Re-entrant auxetic structure geometry

The geometric configuration of re-entrant auxetic cells with length (l), thickness (t), angle (**θ**), and height (h) as shown in the Figure 2. The length of the re-entrant cell is 14.26 mm, thickness 1 mm, angle 30^0 and height 24.7 mm. Three cells with 30^0 angles of re-entrant in one row have been selected as the infill structure of the crash box is presented in Figure 3.

Re-entrant auxetic structures fabricated by 3D printing through FDM technology. Re-entrant auxetic structure printing process with complex geometry is manufactured by depositing layer by layer. The printing material for the 3D printing process is PLA aluminum filament. The filaments manufactured by eSUN. The layer height to manufacture re-entrant auxetic structures was set to 0.1 mm, with an infill density of 100%. The bed temperature was maintained at 40°C, and the printing speed was set to 50 mm/sec. The re-entrant auxetic structure as filler is placed into an aluminum tube of equal length as re-entrant auxetic square tube design (Figure 4). Figure 5 shows the section view of re-entrant auxetic square tube.

Quasi-static compression testing of crash box was conducted using a Tarnogrocky universal testing machine with a capacity of 100 kN, as shown in Figure 6. Force-displacement data were recorded as the samples were compressed between two flat compression plates. The compression was performed at a constant rate of 5 mm/min. The samples were compressed to 100 mm of the 150 mm crash box length.

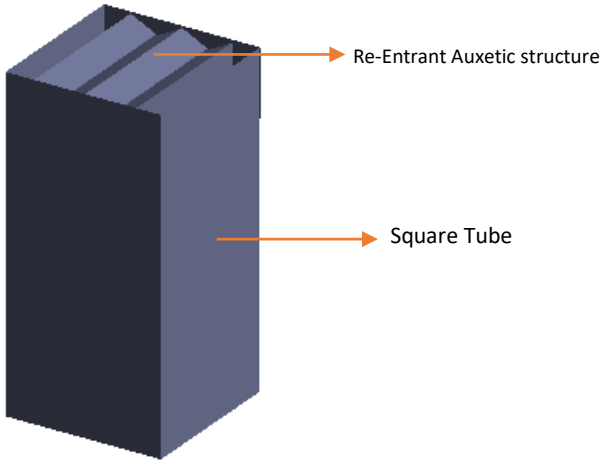

Figure 4. Re-entrant auxetic square tube

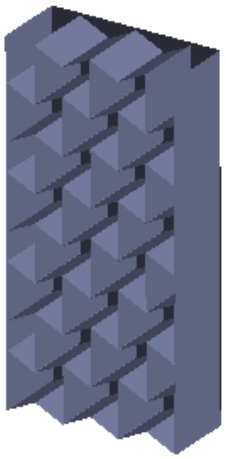

Figure 5. Section view of re-entrant auxetic square tube

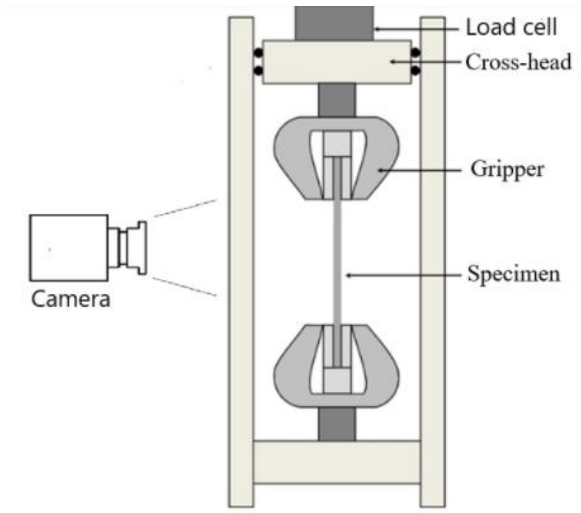

Figure 6. Scematic view of tensile test set up in the Tarnogrocky Universal Testing Machine

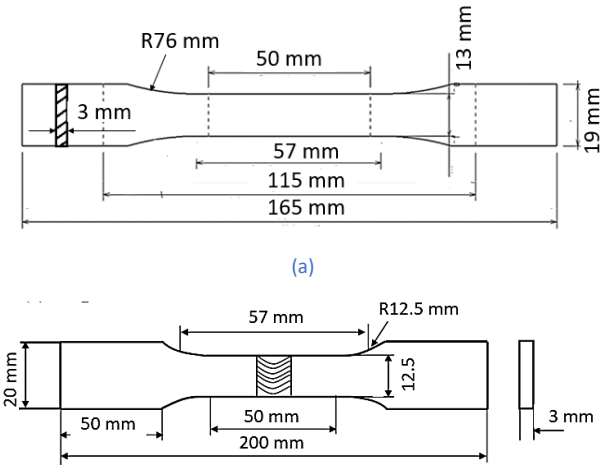

Figure 7. Schematic representation of specimen configuration used for a) PLA Aluminium (ASTM D638), b) Aluminium 6063 (ASTM E-8)

The aluminum tube material and re-entrant auxetic structure were experimentally tested to obtain material property data for simulation. The test conducted was a tensile test using the Tarnogrocki universal testing machine. The tensile test was conducted in accordance with the ASTM E8M standard. The aluminum tensile test specimens are shown in Figure 7 (a). The ASTM D638 standard is used to obtain the tensile test results for PLA-aluminum, as shown in Figure 7 (b). The PLA-aluminum tensile test specimens are 3D printed at a 90° orientation. The material properties of aluminum 6063 are presented in Table 1. The material properties of PLA-aluminum produced by 3D printing are shown in Table 2.

Properties	AL 6063
Density	2700 kg/m^3
Tensile Strength	158.72 MPa
Yield Strength	66.29 MPa
Modulus Elasticity	68.9 GPa
Poisson's Ratio	0.33
Elongation Break	34.7 %

Table 1. Material properties of aluminum 6063

Properties	PLA-ALUMINUM
Density	1280 kg/m^3
Tensile Strength	19.69 MPa
Yield Strength	18.9 MPa
Modulus Elasticity	2.27 GPa
Poisson's Ratio	0.28
Elongation Break	6 %

Table 2. Material properties of PLA aluminium produced 3D Printing

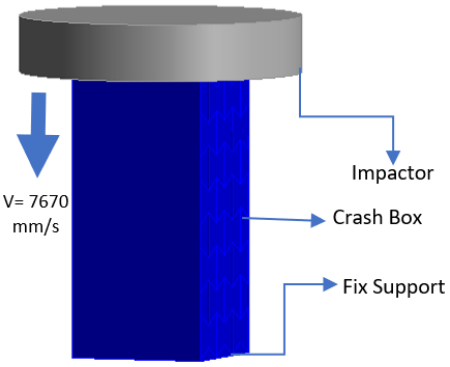

Figure 8. Boundary condition of crash box

The simulation models were constructed using ANSYS 2021 software. The crash box boundary condition is shown in Figure 8. The speed of the impactor is 7670 mm/s. The impactor, with a mass of 103 kg, is assumed to be a rigid based on research by Astuti (2022). The bottom of the crash box is designated as fixed support

EA (Energy Absorption) and SEA (Specific Energy Absorption) are observed as crashworthiness performance. Total energy absorption trough crash box deformation is calculated as the area under the force-displacement curve, using Eq. (1):

$$EA(d) = \int_0^d P(\delta) \quad (1)$$

d is the total crushing distance. P is crushing force and δ is the instantaneous crush displacement.

SEA is the energy absorbed (EA) per unit mass of the crushed test object as shown by the area under the load-displacement curve using Eq. (2).

$$SEA = \frac{energy\ absorbed\ (AE)}{mass\ of\ absorbent\ structure\ (m)} = \int_0^d \frac{P(\delta)}{m} \quad (2)$$

P, δ and m represent the load, displacement and specimen mass, respectively.

3 RESULT AND DISCUSSION

The result of experimental study and simulation are energy absorption and deformation pattern auxetic crash box. A comparison of energy absorption and deformation patterns has been made for each of the square tubes, re-entrant auxetic structures, and re-entrant auxetic square tube.

3.1 Square Tube

The deformation patterns of the square tube, as observed in both experiment and simulation, are shown in Figure 9. Figure 9(a) shows the deformation patterns of a square tube in the experiment. The deformation pattern of the square tube in the

experimental model aligns with the simulation results. Figure 9(b) shows the deformation patterns of a square tube in the simulation. The number of folds produced in the simulation matches with the experiment.

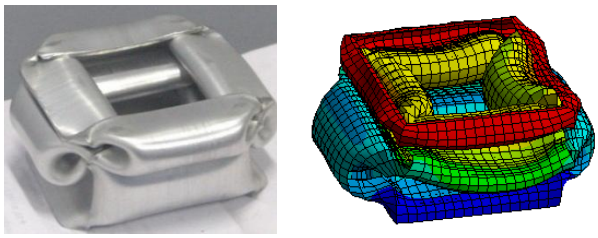

(a) (b)

Figure 9. Deformation pattern of square tube (a) experiment, (b) simulation

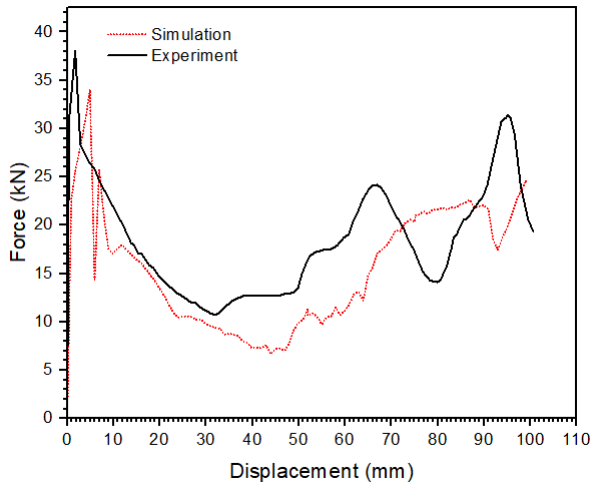

Figure 10. Force-displacement curve of the square tube

The force-displacement curve of the square tube from the experiment and simulation is shown in Figure 10. The initial peak force of the square tube in the experimental and simulation tests shows a slight difference. The initial peak force in the experimental test is higher than in the simulation. This phenomenon is a common occurrence in experimental tests, as presented in the reference (Alavi Nia & Parsapour, 2014). After reaching the peak, the simulated and experiment force-displacement curves exhibit a relatively stable plateau zone. The calculation of the area under the curve to obtain the total energy absorption of the square tube shows an error of only 12.8% between the simulation and the experiment.

Figure 11 presents the crushing process of the square tube in both the simulation and the experiment. The crushing process of the square tube starts from 0 mm to 100 mm (full compression). Figure 13(a) shows the crushing process of a square tube in the experiment. The first fold in the experiment occurred at the center of the square tube. The second fold forms at a displacement of 70 mm. The structure undergoes densification at a displacement of 100 mm, with the folds becoming more compact. Figure 13(b) shows the crushing process of a square tube in the simulation. The first fold in the simulation forms at the top of the square tube, while potential new folds began to develop in the middle of the square tube at a displacement of 35 mm. The second fold and the compaction phase in the simulation form similarly to those in the experiment.

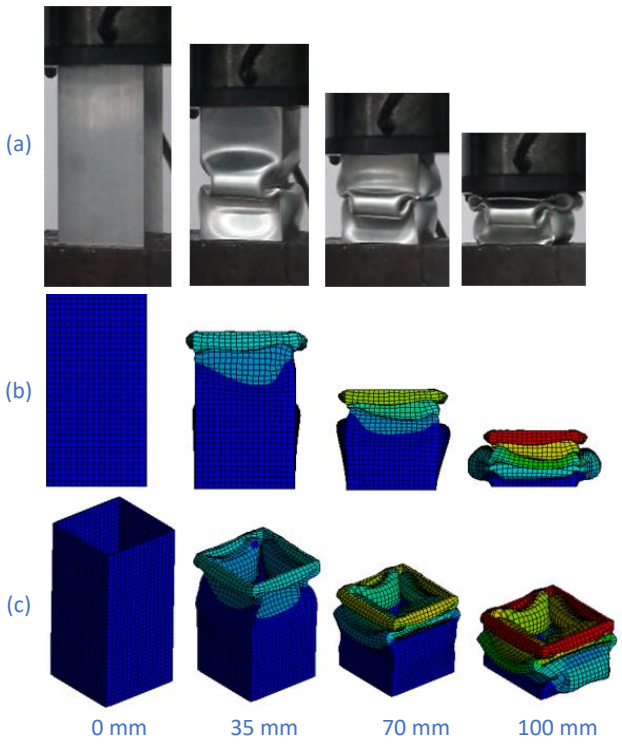

Figure 11. Crushing process of square tube (a) experiment, (b) simulation (c) simulation (Isometric view)

3.2 Re-entrant Auxetic Structure

The deformation patterns of the re-entrant auxetic structure, as observed in experiment and simulation, are shown in Figure 12. Figure 12(a) present the deformation patterns of re-entrant auxetic structure in the experiment. The deformation pattern was observed in the experiment exhibits slight asymmetry. The experimental results show a greater number of re-entrant auxetic folds compared to the simulation. Figure 14 (b) displays the deformation patterns of re-entrant auxetic structure as seen in the simulation. The deformation pattern in the simulation likewise exhibits slight asymmetry.

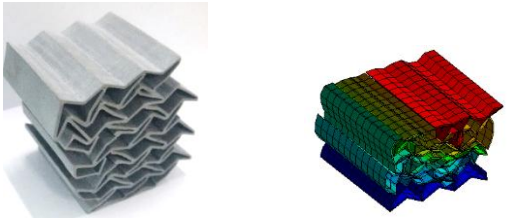

(a) (b)

Figure 12. Deformation pattern of re-entrant auxetic structure (a) experiment, (b) simulation

The force-displacement curve for the re-entrant auxetic structure is shown in Figure 13. The graph illustrates the relationship between force and displacement for the experimentally tested structure (black line) and the simulation (red line). Overall, the patterns of both curves are similar, particularly in the increasing trend of force with displacement. Minor differences are observed at certain points, where the simulation results tend to exhibit higher force peaks than the experimental data. The initial peak force in the experimental test is higher than in the simulation.

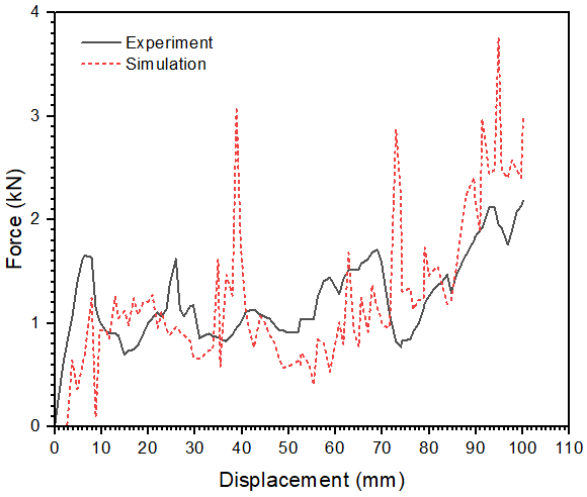

Figure 13. Force-displacement curve of the re-entrant auxetic structure

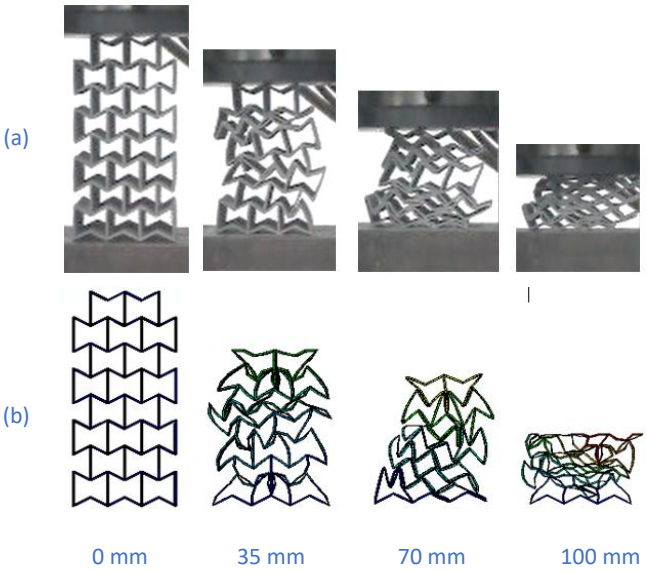

Figure 14. Crushing process of re-entrant auxetic (a) experiment, (b)simulation

The auxetic re-entrant crushing process is shown in Figure 14 (a) for the experiment and Figure 14(b) for the simulation. At a displacement of 35 mm in the experimental test, an initial fold formed at the center of the structure. The first unit cell remains undeformed. At a displacement of 70 mm in the experiment, several folds have formed, exhibiting a more random and progressive folding pattern compared to the simulation. At a displacement of 100 mm in the experiment, the structure becomes more compact, with most unit cells undergoing rightward-tilted deformation. In the simulation at a displacement of 35 mm, the structure begins folding from both the top and bottom toward the center of re-entrant auxetic structure. At a displacement of 70 mm, Figure 14 (b) illustrates the auxetic structure folding to form a square pattern in the center while tilting to the right. At a displacement of 100 mm, Figure 16 (b) shows the structure becoming more compact toward the center.

3.2 Re-entrant Auxetic Square Tube

Figure 15 shows the deformation patterns of the re-entrant auxetic suare tube, as observed in both the experiment and simulation. Figure 15(a) presents the deformation pattern of the auxetic re-entrant square tube observed during experimental testing, while Figure 15(b) shows the corresponding deformation pattern from the simulation results. The deformation patterns of both models show almost uniform patterns. The number of folds in the re-entrant auxetic square tube increases during the deformation process. The increased number of folds enables the re-entrant auxetic square tube to absorb more energy during compression

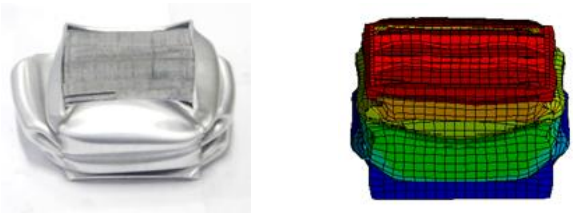

(a) (b)

FiFigure 15. Deformation pattern of re-entrant auxetic square tube (a) experiment, (b) simulation

Figure 16 shows Force-displacement curve of re-entrant auxetic square tube. The peak force in both tests is nearly identical, recorded at 38.74 kN for the experiment and 39.37 kN for the simulation, respectively. During the elastic deformation stage of the re-entrant auxetic square tube in the experiment, the force rapidly increases before decreasing. The next deformation change the plastic stage. The force continues to increase until the end of the loading process. In the simulation, after reaching the peak force, the force decreases rapidly and then fluctuates consistently until the end of the loading process.

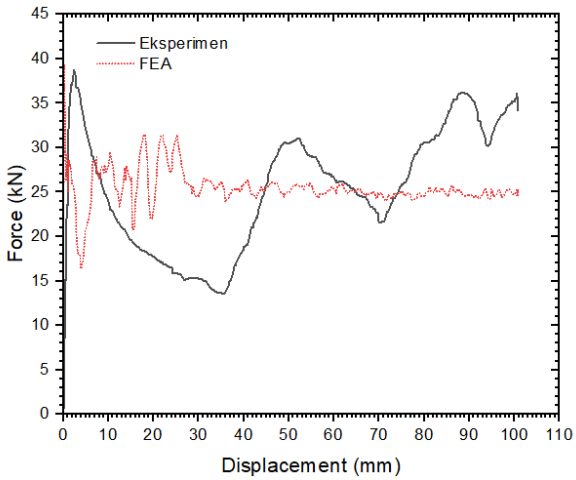

Figure 16. Force-displacement curve of re-entrant auxetic square tube

Figure 17 (a) presents the crushing process of the re-entrant auxetic square tube observed in the experiment. At a displacement of 35 mm, initial folding occurs in the middle of the crash box. As the displacement increases to 70 mm, the deformation becomes more pronounced, with the central region of the tube exhibiting more complex folding due to compressive forces. At a displacement of 100 mm, the structure reaches its final deformation stage, with the tube nearly fully compressed.

Figure 19(b) presents the crushing process of the re-entrant auxetic square tube in the simulation. At a displacement of 35 mm, the structure begins to undergo initial deformation due to compressive forces, with the first folding at the top of the tube. At a displacement of 70 mm, the deformation becomes more pronounced, and the central region of the tube exhibits a more complex folding. By a displacement of 100 mm, the structure has reached the densification stage.

Figure 19 (c) presents an isometric view of the deformation of the re-entrant auxetic square tube structure in the simulation. At a displacement of 35 mm, the auxetic structure begins to fold from the top, while the lower and middle sections remain unchanged. At a displacement of 70 mm, the deformation pattern progresses in a controlled manner, continuing until the end of the loading process.

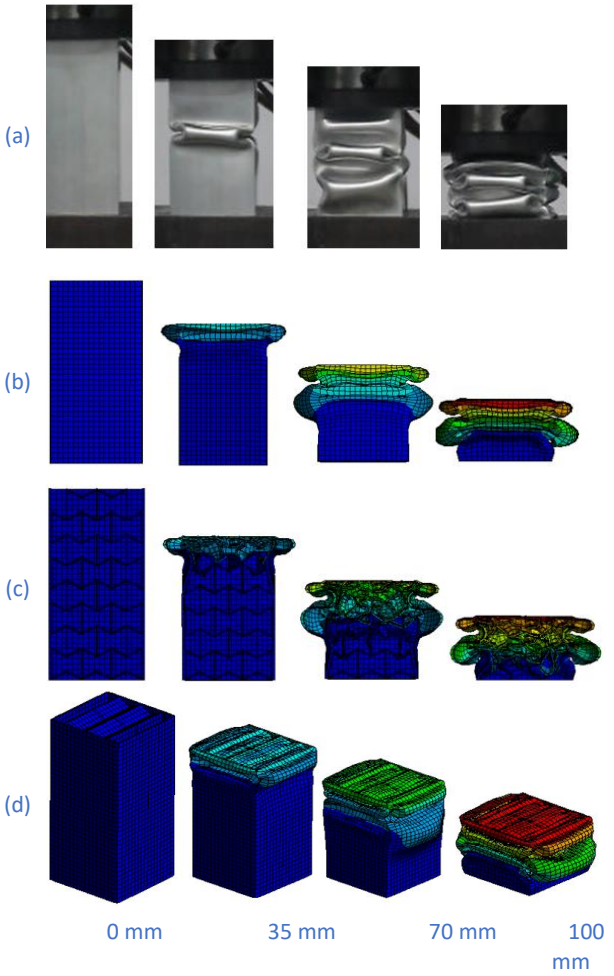

Figure 17. Crushing process of re-entrant auxetic square tube (a) Experimental, (b) simulation, (c) simulation (section), (d) simulation (isometric view)

Figure 18 provides a comparative overview of energy absorption (EA) in Figure 18 (a) and specific energy absorption (SEA) in Figure 18 (b) for the square structure, re-entrant auxetic structure, and re-entrant auxetic square tube. The data is presented using two approaches simulation results and experimental results. These three configurations exhibit different performances in energy absorption, offering valuable insights for the design of crash boxes and other energy-absorbing structures.

For the square tube, the EA value obtained from the simulation is 1.529 kJ, while the experimental result is 1.723 kJ. The experimental value is slightly higher than the simulation, reflecting the actual conditions observed during testing. The empty square tube serves as a crucial baseline for comparison with other configurations, as it represents the fundamental structural characteristics without additional modifications.

The re-entrant auxetic structure exhibits a significantly lower EA value compared to the square tube. Although the re-entrant auxetic structure possesses unique mechanical properties, such as a negative Poisson's ratio, it is unable to effectively absorb energy when used independently. This limitation is likely due to its low structural stiffness, which restricts the amount of energy absorbed during the deformation process. In both the simulation and the experiment, the EA values of the re-entrant auxetic structure are nearly identical, indicating that the simulation accurately represents the characteristics of this auxetic structure.

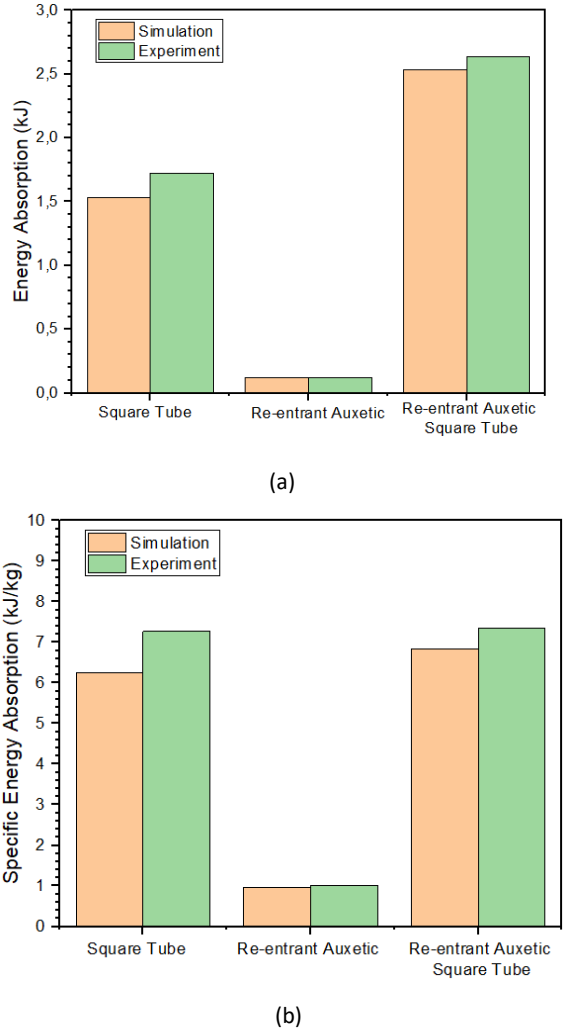

Figure 18. Comparison between all models for (a) energy absorption and (b) specific energy absorption.

The re-entrant auxetic square tube which consists of a square tube with a re-entrant auxetic structure, yields highly promising results. Among the three tested configurations, this re-entrant auxetic square tube achieves the highest EA values in both the simulation (2.534 kJ) and the experiment (2.637 kJ). The exceptional performance of re-entrant auxetic square tube suggests a synergistic interaction between the square tube and the re-entrant auxetic structure. The presence of the auxetic structure inside the tube may enhance local stiffness and facilitate a more uniform force distribution during the

deformation process, thereby increasing overall energy absorption capacity.

The SEA values for the square tube in the experimental and simulation tests are 7.270 kJ/kg and 6.241 kJ/kg, respectively. The SEA values for the re-entrant auxetic structure in the experimental and simulation tests are 1.006 kJ/kg and 0.961 kJ/kg. Meanwhile, the SEA values for the re-entrant auxetic square tube in the experimental and simulation tests are 7.36 kJ/kg and 6.83 kJ/kg. The square tube, re-entrant auxetic, and re-entrant auxetic square tube exhibit the same trend in energy absorption (EA) and specific energy absorption (SEA) between simulation and experimental results. The specific energy absorption (SEA) of the re-entrant auxetic structure increased significantly compared to the square tube, with an increase of 1.24% and 9.47% in the experimental and simulation results, respectively.

In the experiment, the EA value was increased by 53.047% when comparing the square tube to the re-entrant auxetic square tube. The addition of re-entrant auxetic structures enhances energy absorption capability (Simpson & Kazancı, 2020). Notably, the EA the re-entrant auxetic square tube not only approached the sum of the EA values of the square tube and the re-entrant auxetic structure but also exceeded it. This phenomenon highlights the additional benefits obtained from the combination of these structures, which cannot be achieved when either the empty square tube or the re-entrant auxetic structure is used separately.

CONCLUSIONS

In this study, the crashworthiness performance of an empty square tube, a re-entrant auxetic structure, and a crash box filled with a re-entrant auxetic structure under quasi-static compressive loading was investigated. To achieve this, the re-entrant auxetic-filled tubes are compared with a re-entrant auxetic structure and an empty square tube. Through the development of a simulation model and experimental validation tests, it was observed that the addition of re-entrant auxetic structures significantly enhanced the crashworthiness performance of the re-entrant auxetic square tube compared to the empty square tube. Based on experimental energy absorption (EA) values, the inclusion of a re-entrant auxetic filler resulted in a 53.047% increase over the empty square tube. This improvement corresponds to a 1.23% increase in specific energy absorption (SEA). The energy absorption characteristics of the re-entrant auxetic-filled square tube are superior to those of the empty square tube. Furthermore, the combination of the re-entrant auxetic structure with the square tube provides additional benefits that are not achievable when using either the empty square tube or the re-entrant auxetic structure individually.

ACKNOWLEDGMENTS

The authors would like to acknowledge the support of Design and System Engineering Laboratory, Brawijaya University for ANSYS Research license facilities. This research was funded by Professor's Scheme Grant of Engineering Faculty 2023, Brawijaya University, Indonesia.

REFERENCES

[Airoldi 2020] Airoldi, A., Novak, N., Sgobba, F., Gilardelli, A., & Borovinšek, M. (2020). Foam-filled energy absorbers with auxetic behaviour for localized impacts. *Materials Science and Engineering A*, *788*(May). https://doi.org/10.1016/j.msea.2020.139500

[Alavi 2014] Alavi Nia, A., & Parsapour, M. (2014). Comparative analysis of energy absorption capacity of simple and multi-cell thin-walled tubes with triangular, square, hexagonal and octagonal sections. *Thin-Walled Structures*, *74*, 155–165. https://doi.org/10.1016/j.tws.2013.10.005

[Astuti 2023] Astuti, F. A. F., Choiron, M. A., Purnowidodo, A., & Irawan, Y. S. (2023). Multi-Objective Design of Honeycomb Hybrid Crash Box Under Frontal Loading. *MM Science Journal*, *2023-March*, 6413–6420. https://doi.org/10.17973/MMSJ.2023_03_2022162

[Dhari 2021] Dhari, R. S., Javanbakht, Z., & Hall, W. (2021). On the inclined static loading of honeycomb re-entrant auxetics. *Composite Structures*, *273*(May), 114289. https://doi.org/10.1016/j.compstruct.2021.114289

[Evans 1991] Evans, K. E. (1991). Auxetic polymers: a new range of materials. *Endeavour*, *15*(4), 170–174. https://doi.org/10.1016/0160-9327(91)90123-S

[Fang 2015] Fang, J., Gao, Y., Sun, G., Zheng, G., & Li, Q. (2015). Dynamic crashing behavior of new extrudable multi-cell tubes with a functionally graded thickness. *International Journal of Mechanical Sciences*, *103*(May 2021), 63–73. https://doi.org/10.1016/j.ijmecsci.2015.08.029

[Ghiasvand 2023] Ghiasvand, A., Khanigi, A. F., Guerrero, J. W. G., Derazkola, H. A., Tomków, J., Janeczek, A., & Wolski, A. (2023). Investigating the Effects of Geometrical Parameters of Re-Entrant Cells of Aluminum 7075-T651 Auxetic Structures on Fatigue Life. *Coatings*, *13*(2). https://doi.org/10.3390/coatings13020405

[Günayd 2019] Günayd, K., Eren, Z., Kazanc, Z., & Scarpa, F. (2019). *In-plane compression behavior of anti- tetrachiral and re-entrant lattices*.

[Huang 2017] Huang, J., Zhang, Q., Scarpa, F., Liu, Y., & Leng, J. (2017). In-plane elasticity of a novel auxetic honeycomb design. *Composites Part B: Engineering*, *110*, 72–82. https://doi.org/10.1016/j.compositesb.2016.11.011

[Ju 2011] Ju, J., & Summers, J. D. (2011). Compliant hexagonal periodic lattice structures having both high shear strength and high shear strain. *Materials and Design*, *32*(2), 512–524. https://doi.org/10.1016/j.matdes.2010.08.029

[Li 2019] Li, X., Wang, Q., Yang, Z., & Lu, Z. (2019). Novel auxetic structures with enhanced mechanical properties. *Extreme Mechanics Letters*, *27*, 59–65. https://doi.org/10.1016/j.eml.2019.01.002

[Lian 2023] Lian, J., & Wang, Z. (2023). Impact Response of Re-Entrant Hierarchical Honeycomb. *Materials*, *16*(22). https://doi.org/10.3390/ma16227121

[Liu 2021] Liu, H., Chng, Z. X. C., Wang, G., & Ng, B. F. (2021). Crashworthiness improvements of multi-cell thin-walled tubes through lattice structure enhancements. *International Journal of Mechanical Sciences*, *210*(May), 106731. https://doi.org/10.1016/j.ijmecsci.2021.106731

[Liu 2016] Liu, W., Wang, N., Luo, T., & Lin, Z. (2016). In-plane dynamic crushing of re-entrant auxetic cellular structure. *Materials and Design*, *100*, 84–91.

https://doi.org/10.1016/j.matdes.2016.03.086

[Mauko 2021] Mauko, A., Fíla, T., Falta, J., Koudelka, P., Rada, V., Neuhäuserová, M., Zlámal, P., Vesenjak, M., Jiroušek, O., & Ren, Z. (2021). Dynamic deformation behaviour of chiral auxetic lattices at low and high strain-rates. *Metals*, *11*(1), 1–15. https://doi.org/10.3390/met11010052

[Meena 2019] Meena, K., & Singamneni, S. (2019). A new auxetic structure with significantly reduced stress concentration effects. *Materials and Design*, *173*, 107779. https://doi.org/10.1016/j.matdes.2019.107779

[Rad 2015] Rad, M. S. (2015). *Auxetic Structures for Energy Absorption Applications*. *June*.

[Shruti 2020] Shruti, M., Hemanth, N. S., Badgayan, N. D., & Sahu, S. K. (2020). Compressive behavior of auxetic structural metamaterial for lightweight construction using ANSYS static structural analysis. *Materials Today: Proceedings*, *38*, 12–17. https://doi.org/10.1016/j.matpr.2020.05.410

[Simpson 2020] Simpson, J., & Kazancı, Z. (2020). Crushing investigation of crash boxes filled with honeycomb and re-entrant (auxetic) lattices. *Thin-Walled Structures*, *150*(February), 106676. https://doi.org/10.1016/j.tws.2020.106676

[Song 2022] Song, J., Xu, S., Liu, S., & Zou, M. (2022). Study on the crashworthiness of bio-inspired multi-cell tube under axial impact. *International Journal of Crashworthiness*, *27*(2), 390–399. https://doi.org/10.1080/13588265.2020.1807686

[Wang 2020] Wang, J., Xiang, J., Lin, H., Wang, K., Yao, S., Peng, Y., & Rao, Y. (2020). Effects of scanning strategy and printing temperature on the compressive behaviors of 3D printed polyamide-based composites. *Polymers*, *12*(8). https://doi.org/10.3390/polym12081783

[Wang 2022] Wang, K., Liu, Y., Wang, J., Xiang, J., Yao, S., & Peng, Y. (2022). On crashworthiness behaviors of 3D printed multi-cell filled thin-walled structures. *Engineering Structures*, *254*(October 2021). https://doi.org/10.1016/j.engstruct.2022.113907

[Wang 2017] Wang, X. T., Wang, B., Li, X. W., & Ma, L. (2017). Mechanical properties of 3D re-entrant auxetic cellular structures. *International Journal of Mechanical Sciences*, *131–132*(July), 396–407. https://doi.org/10.1016/j.ijmecsci.2017.05.048

[Warner 2017] Warner, J. J., Gillies, A. R., Hwang, H. H., Zhang, H., Lieber, R. L., & Chen, S. (2017). 3D-printed biomaterials with regional auxetic properties. *Journal of the Mechanical Behavior of Biomedical Materials*, *76*(March), 145–152. https://doi.org/10.1016/j.jmbbm.2017.05.016

[Yang 2021] Yang, H., & Ma, L. (2021). Impact resistance of additively manufactured 3D double-U auxetic structures. *Thin-Walled Structures*, *169*(February). https://doi.org/10.1016/j.tws.2021.108373

[Zhao 2018] Zhao, X., Gao, Q., Wang, L., Yu, Q., & Ma, Z. D. (2018). Dynamic crushing of double-arrowed auxetic structure under impact loading. *Materials and Design*, *160*, 527–537. https://doi.org/10.1016/j.matdes.2018.09.041